Research Square

Preprints are preliminary reports that have not undergone peer review.
They should not be considered conclusive, used to inform clinical practice,
or referenced by the media as validated information.

# Chest Computed Tomography Habitat and Body Composition for Survival Prediction in Stage IV Lung Cancer

**peiqi wang**
Panzhihua Traditional Chinese Medicine and Western Medicine Hospital
**Hao Hu**
Kunming Medical University Affiliated Calmette Hospital
**Yubo Wang**
Kunming Medical University Affiliated Calmette Hospital
**Yadan Yin**
Kunming Medical University Affiliated Calmette Hospital
**Yang Fu**
Kunming Medical University Affiliated Calmette Hospital
**Bosen Xie**
Kunming Medical University Affiliated Calmette Hospital
**Jiageng Li**
Kunming Medical University Affiliated Calmette Hospital
**Mengxue Kong**
Kunming Medical University Affiliated Calmette Hospital
**Chunyuan Wei**
Kunming Medical University Affiliated Calmette Hospital
**Lei Yue**
Panzhihua Central Hospital
**Duiming Yang**
Baoshan Second People's Hospital
**Bin Yang**
yangbinapple@163.com

Kunming Medical University Affiliated Calmette Hospital

**Research Article**

**Keywords:** CT imaging, non-small cell lung cancer, radiomics, habitat imaging, body composition analysis, survival prediction

**Posted Date:** November 18th, 2026

**DOI:** https://doi.org/10.21203/rs.3.rs-11442726/v1

**License:** This work is licensed under a Creative Commons Attribution 4.0 International License.
Read Full License

**Additional Declarations:** No competing interests reported.

# Chest Computed Tomography Habitat and Body Composition for Survival Prediction in Stage IV Lung Cancer


## Author names

Peiqi Wang[1#], Hao Hu[2,3#],Yubo Wang[2,3#], Yadan Yin[2,3#],Yang Fu[2#], Bosen Xie[2], Jiageng Li[2],Mengxue Kong[2], Chunyuan Wei[2], Lei Yue[4],Duiming Yang[5]*,Bin Yang[2,3]*

[#]Peiqi Wang, Hao Hu, Yubo Wang, Yadan Yin and Yang Fu contributed equally to this work.

## Affiliations

1.Department of Medical Imaging,Panzhihua Traditional Chinese Medicine and Western Medicine Hospital,Panzhihua,617000,China

2.Department of Medical Imaging,Kunming Medical University Affiliated Calmette Hospital, Kunming, 650051, China

3.Kunming Medical University, Kunming, 650500, China

4.Department of Medical Imaging,Panzhihua Central Hospital, Panzhihua, 617000, China

5.Department of Medical Imaging,Baoshan Second People's Hospital, Baoshan,Yunnan 678000, China

## Corresponding author

*Corresponding author: Dr. BinYang. E-mail: yangbinapple@163.com.

*Co-corresponding author: Dr. Duiming Yang. E-mail: 17347083@qq.com

**Abstract**

**Objectives:** To integrate clinical characteristics, CT habitat radiomic features, and quantitative body composition parameters in patients with stage IV non-small-cell lung cancer (NSCLC) and develop a multidimensional model for predicting overall survival.

**Materials and methods:** Overall, 196 patients with stage IV NSCLC were retrospectively enrolled and divided into a training set (n = 137) and an internal test set (n = 59). An additional 50 patients formed an external test set. Radiomic features of the entire tumor, tumor habitat features based on K-means clustering, and body composition at the L3 vertebral level were extracted using 3D Slicer. Random forest and LASSO(LASSO) regression were utilized for feature selection, followed by the construction of unimodal, bimodal, and multi-dimensional integrated prognostic models. Model performance was evaluated via Harrell's concordance index, time-dependent receiver operating characteristic (ROC) curves, and Kaplan–Meier survival analysis. The SHapley Additive exPlanations (SHAP) method was used for model interpretability analysis.

**Results:** The multidimensional fusion model achieved the best performance, with area under the curve values of 0.842, 0.811, and 0.817 in the training, internal, and external test sets, respectively. It significantly outperformed single-modality models and effectively stratified patients into high- and low-risk groups (log-rank p = 0.00067). C-indices were 0.850, 0.790, and 0.760, respectively. SHAP analysis identified body composition features as key contributors to survival

prediction.

**Conclusion:** The proposed model demonstrated robust prognostic performance and may support individualized management of advanced NSCLC.

**Keywords:** CT imaging; non-small cell lung cancer; radiomics; habitat imaging; body composition analysis; survival prediction

## 1 Introduction

Lung cancer is one of the most prevalent malignancies worldwide. Non-small-cell lung cancer (NSCLC) accounts for approximately 85–90% of all cases [1-3]. Despite major therapeutic advances in immune checkpoint inhibitors and targeted therapies[4-6], overall survival (OS) in stage IV non-small-cell lung cancer (NSCLC) remains highly heterogeneous. A key unresolved scientific question is why patients with similar clinical stage, molecular characteristics, and treatment regimens exhibit markedly different survival outcomes, suggesting that current prognostic systems incompletely capture disease biology.

Existing prognostic frameworks rely primarily on TNM staging and single-molecule biomarkers such as programmed death-ligand 1 (PD-L1). However, TNM staging reflects only anatomical tumor burden and does not capture biological behavior, while biomarkers are limited by sampling bias, spatial heterogeneity, and temporal variability [7,8]. This creates a critical gap in accurately stratifying patients with advanced disease.

Intratumoral heterogeneity (ITH) has been identified as a major driver of therapeutic resistance and survival variability [9]. Radiomics provides noninvasive quantification of tumor heterogeneity and has demonstrated prognostic value [10,11]. More recently, habitat imaging has enabled decomposition of tumors into spatially distinct functional subregions, improving assessment of ITH and enhancing prediction of immunotherapy response, pathological aggressiveness, and immune infiltration patterns [12-16]. However, most radiomic approaches remain tumor-centric and ignore host biological factors.

Host-related conditions such as cachexia and sarcopenia are also strongly associated with treatment tolerance and survival in advanced NSCLC [17,18]. Computed tomography (CT)-based body composition analysis (BCA) enables objective quantification of skeletal muscle and adipose tissue, reflecting systemic nutritional and metabolic status [19-22]. With the rapid advancement of deep learning and multi-omics technologies, the integration of multimodal data has become an inevitable trend in prognostic research [23,24]. However, a critical unmet need persists in this field: most existing models focus solely on tumor-derived imaging/molecular features or host-related inflammatory/metabolic indicators. Few studies have systematically integrated habitat features (reflecting tumor spatial heterogeneity) and body composition features (representing host tolerance) within a unified predictive framework for stage IV NSCLC [25,26]. Single-dimensional assessment often fails to explain the drastically divergent survival trajectories observed in patients with similar clinical staging and genotypic profiles

(e.g., subtypes revealed by multiple instance learning or dynamic circulating tumor DNA (ctDNA) monitoring) [27-31]..

To address this gap, we propose a holistic "tumor–host" prognostic framework that integrates CT-based habitat radiomic features, quantitative body composition parameters, radiomic scores, and clinicopathological variables. This model aims to provide a noninvasive, interpretable tool for individualized OS prediction and improved risk stratification in stage IV NSCLC.

## 2 Materials and methods

### 2.1 Study population

This retrospective study was approved by the ethics committee, and the requirement for informed consent was waived (ethics approval No. PCWEC-C-005). The clinical data of 196 patients with stage IV NSCLC treated at Panzhihua Traditional Chinese Medicine and Western Medicine Hospital from January 2015 to January 2021 were retrospectively collected. The patients were randomly divided in a 7:3 ratio into a training set (n=137) and an internal test set (n=59). Demographic information (age, sex, smoking history, family history), laboratory tests (AFP, CEA, CA125, CA199, NSE, SCC), and pathological findings (tumor type, EGFR, PD-L1) were extracted from electronic medical records. The tumor location and TNM stage (AJCC 9th edition) were also recorded. Additionally, data from 50 patients with stage IV NSCLC at Panzhihua Central Hospital were retrospectively collected as an external test set.

The inclusion criteria were as follows: (1) age ＞18 years, (2) pathologically confirmed NSCLC, (3) the presence of one or more distant metastases, and (4) complete clinical data. The exclusion criteria were as follows: (1) other concurrent malignancies, (2) concurrent diffuse pulmonary diseases (e.g., tuberculosis and silicosis), and (3) prior neoadjuvant chemoradiotherapy or molecular targeted therapy before enrollment.

## 2.2 Outcome definition and survival stratification

OS was the primary endpoint, defined as the time from the initial diagnosis of stage IV NSCLC to death from any cause or the last effective follow-up. Because OS is a time-to-event outcome and censored observations cannot be appropriately handled by multinomial logistic regression, OS was analyzed primarily using Cox proportional hazards models. Patients were additionally categorized into short-term (OS ⩽ 1 year), medium-term (1 year < OS ⩽ 3 years), and long-term (OS > 3 years) groups for descriptive purposes only. These categories were not used as the primary dependent variable in the main prognostic models.

## 2.3 CT image acquisition and feature extraction

### 2.3.1 Chest CT scanning

All patients were scanned from the thoracic inlet to the diaphragmatic base in the supine position. Parameters: slice thickness 5.0 mm, tube voltage 120

kVp, automatic tube current modulation, reconstruction kernel B70f, reconstructi on thickness 1.0 mm, and standard lung window (width 1200 HU, level –600 HU).

### 2.3.2 Upper abdominal CT scanning

Supine position from the diaphragmatic base to the iliac crest level. The p arameters were as follows: slice thickness 5.0 mm, tube voltage 120 kVp; auto matic tube current; reconstruction kernel B30f; reconstruction thickness 1.0 mm, and standard soft-tissue window (width, 450 HU; level, 40 HU).

### 2.3.3 Radiomics feature extraction

DICOM images were stored and imported into 3D Slicer (version 5.8.1). Voxel sizes were standardized by interpolation prior to feature extraction. A rad iologist with 8 years of experience in chest imaging manually delineated the tu mor region of interest (ROI) on lung window images, slice by slice. The delin eation was repeated one month later, and the intraclass correlation coefficient (I CC) between the two sets was calculated, with ICC $\geq$ 0.85 considered reliable. Overall, 107 radiomic features were extracted using the SlicerRadiomics modu le. These features are collectively referred to as radiomics (RS) features.

### 2.3.4 Habitat feature extraction

Habitat segmentation was performed within 3D Slicer (5.8.1) using the pre

viously delineated white tumor ROI. Voxel-wise gray-level intensity and first-order texture features were extracted. Gray values were normalized to the range [–1000, 400] HU to eliminate scanner-related variations. K-means clustering (K = 4, determined by the CH index) was applied to partition the tumor into four habitat subregions, each representing a set of voxels with similar intensity and texture characteristics. Radiomic features were then extracted from each habitat subregion using the same feature categories and parameters as those for the entire tumor ROI. In addition, the following habitat-related quantitative metrics were calculated: (1) volume fraction of each habitat; (2) internal radiomic features of each habitat; (3) inter-habitat heterogeneity indices (e.g., gray-level differences, texture dispersion, volume proportion balance). These features are collectively called ITH.

### 2.3.5 Body composition feature extraction

DICOM images were imported into 3D Slicer (5.8.1). A radiologist with 8 years of abdominal imaging experience manually delineated the subcutaneous adipose tissue, intermuscular adipose tissue (IMAT), visceral adipose tissue, and skeletal muscle at the L3 vertebral level on soft-tissue window images. The first-order and textural features were extracted from each region. These features are collectively referred to as BCA features.

## 2.4 Feature selection

To avoid overfitting and multicollinearity, different selection strategies were applied to the clinical features RS, ITH, and BCA.

Clinical features: Random forest was used to rank feature importance for the three-class outcomes, and significant contributors were selected for subsequent clinical and combined models.

RS, ITH, and BCA features: Least absolute shrinkage and selection operator (LASSO) regression with L1 penalty was applied separately to each feature set. The optimal λ was determined by ten-fold cross-validation, and features with non-zero coefficients were retained.

## 2.5 Model construction

Because OS is a time-to-event endpoint, all primary models were constructed using Cox proportional hazards regression rather than multinomial logistic regression. Clinical variables were preselected using random forest importance ranking and univariate Cox analysis. RS, ITH, and BCA features were separately subjected to least absolute shrinkage and selection operator (LASSO) with an L1 penalty under a Cox framework. The optimal penalty parameter λ was determined by ten-fold cross-validation within the training set, and features with non-zero coefficients were retained.

We constructed 10 Cox models corresponding to the same feature dimensions as originally planned:

(1) single-modality models: Clinical, RS, ITH, and BCA;

(2) two-modality models: Clinical + RS, Clinical + ITH, Clinical + BCA, and RS + ITH;

(3) multi-modality models: RS + ITH + BCA and Clinical + RS + ITH + BCA.

The proportional hazards assumption was checked using Schoenfeld residuals. The linear predictor from each Cox model was used as the risk score. Patients were stratified into high- and low-risk groups using the median risk score or a maximally selected rank statistic in the training set, and the same cutoff was applied to the internal and external test sets.

### 2.6 Model validation

Internal validation was performed using five-fold cross-validation and bootstrap resampling (1000 replicates) within the training set to estimate optimism-corrected performance. Generalization was evaluated using an independent internal test set (n = 59) and an external test set (n = 50). Because the external cohort was relatively small, external validation was considered exploratory, and confidence intervals were reported.

### 2.7 Model evaluation

Model discrimination was assessed using Harrell’s concordance index (C-index) for Cox models. Time-dependent receiver operating characteristic (ROC) curves were generated using Heagerty’s method, and time-dependent AUCs we

re calculated at 1, 3, and 5 years. The C-index and time-dependent AUC are conceptually different: the C-index summarizes global rank discrimination over the entire follow-up period, whereas time-dependent AUC evaluates discrimination at a specific time point. Therefore, they are reported separately and should not be expected to be identical.

Calibration was evaluated using calibration curves and the Brier score. Kaplan–Meier survival curves and log-rank tests were used to compare high- and low-risk groups. Decision curve analysis was used to assess clinical utility.

### 2.7.1 Classification discrimination

Macro-average AUC: For the three-class problem, we computed the one-vs-Rest AUC for each pair and averaged them, with 95% confidence intervals estimated.

Accuracy (ACC), macro-average sensitivity (macro-SEN), macro-average specificity (macro-SPE), and macro-average F1-score (macro-F1).

### 2.7.2 Survival stratification

Based on the model-predicted class (short-/medium-/long-term), patients were re-classified into “high-risk” (predicted short-term) and “low-risk” (predicted medium- or long-term) groups. Kaplan–Meier survival curves and log-rank tests were used to evaluate the model’s ability to discriminate actual OS differences between risk groups. In addition, time-dependent receiver operating characteris

tic (ROC) curves (Heagerty's method) were plotted to assess the accuracy of the model in predicting long-term survival (OS > 3 years) at the 3-year time point.

### 2.8 SHAP interpretability analysis

For the full-dimensional Cox model, SHAP (SHapley Additive exPlanations) was used to quantify the contribution and direction of each feature. A positive SHAP value indicated a push toward higher risk, whereas a negative value indicated lower risk. Feature importance bar plots and beeswarm plots were generated. The three-category OS groups were used only to aid descriptive interpretation and not as the primary modeling outcome.

The overall workflow is illustrated in Figure 1.

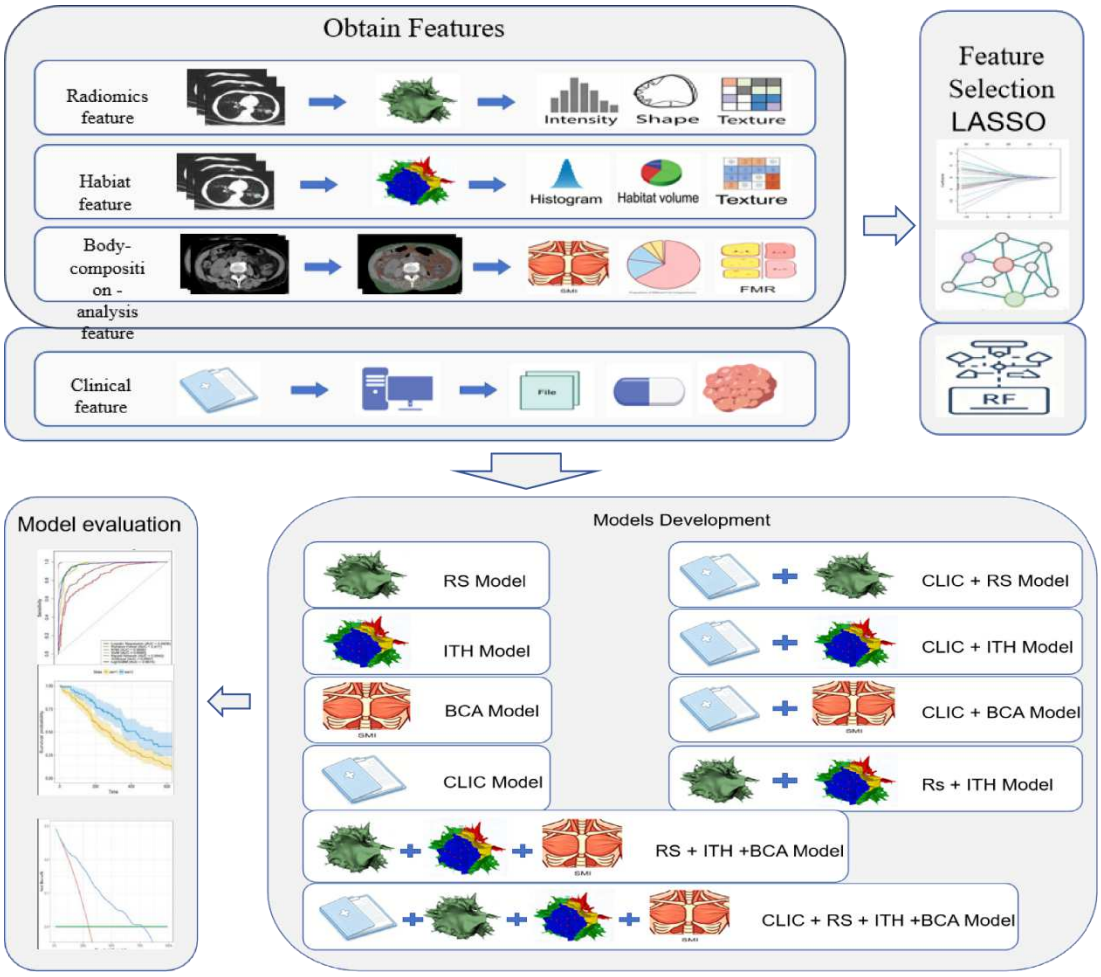



**Figure 1. Overall workflow of the study**

## 3 Results

### 3.1 Clinical feature selection results

The random forest importance ranking (Figure 2) showed that age (importance score 0.133) was the most important predictor, followed by NSE (0.120), CEA (0.119), SCC (0.091), Ki-67 (0.079), treatment method (0.075), and tumor location (0.059). TNM stage, metastatic sites, smoking history, EGFR status, and other factors had scores below 0.05.

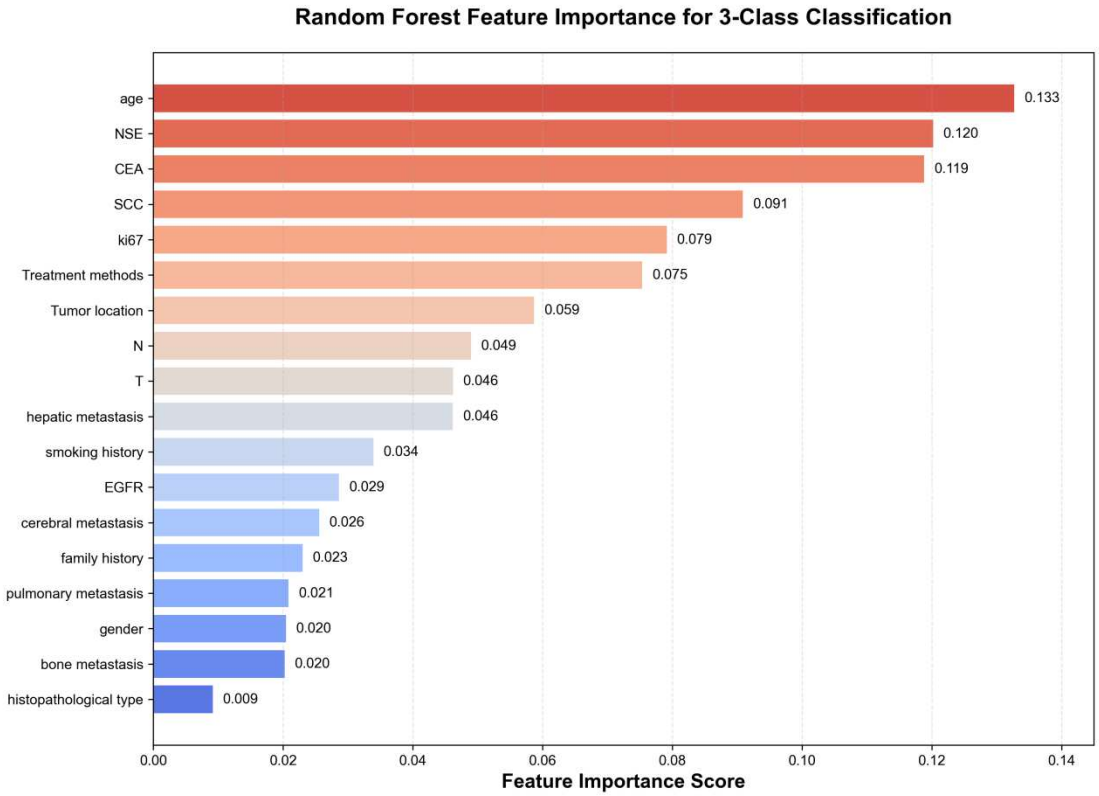



**Figure 2. Ranking plot of the contribution degrees of clinical and pathological features to model classification decisions**

### 3.2 Multi-dimensional Feature Selection Results

The LASSO regression selected three, eight, and seven non-zero-coefficient features from RS, ITH, and BCA, respectively (detailed in Table 1). ITH features were predominantly texture features (GLCM/GLRLM), while BCA features included texture and shape features from the fat and muscle regions. The coefficients and their corresponding directions are presented in Table 1.

**Table 1. Key feature coefficients derived from LASSO regression**

| Source | Feature | Coefficient |
|---|---|---|
| RS | original_shape_Sphericity_ALL | 0.11672711172759886 |

| Source | Feature | Coefficient |
|---|---|---|
| ITH | original_ngtdm_Coarseness_ALL | 0.027451596861751814 |
| | original_firstorder_90Percentile_ALL | -0.11641087 |
| | original_glszm_GrayLevelNonUniformityNormalized_Se | 0.06894750125237212 |
| | original_glszm_SmallAreaLowGrayLevelEmphasis_Se | 0.01723278333632049 |
| | original_shape_SurfaceVolumeRatio_Se | 0.061451559679895566 |
| | original_glcm_ClusterShade_Fo | -0.063800714 |
| | original_gldm_SmallDependenceEmphasis_Fo | 0.0771299697382056 |
| | original_glrlm_RunLengthNonUniformityNormalized_Th | 0.028005515592340605 |
| | original_firstorder_90Percentile_Fi | -0.016016767 |
| | original_shape_Maximum2DDiameterColumn_Fi | 0.010458306437642634 |
| BCA | original_firstorder_Kurtosis_VAT | 0.16961426065447627 |
| | original_glszm_ZonePercentage_SAT | 0.12790120465055077 |
| | original_glcm_ClusterProminence_IMAT | 0.1099170179044899 |
| | original_shape_Maximum2DDiameterSlice_IMAT | 0.08549002281911218 |
| | original_shape_Maximum3DDiameter_IMAT | 0.000000167746 |
| | original_glszm_SizeZoneNonUniformityNormalized_IMAT | -0.142387354 |
| | original_glcm_DifferenceEntropy_SAT | 0.005438891087291956 |

**Abbreviations:** LASSO, least absolute shrinkage and selection operator; RS, radiomics score (radiomic signature); ITH, intratumoral heterogeneity; BCA, body composition analysis; SAT, subcutaneous adipose tissue; IMAT, intermuscular adipose tissue; VAT, visceral adipose tissue.

### 3.3 Model performance

The classification performances of the 10 models are summarized in Table 2. The full-dimensional fusion model (Clinical + RS + ITH + BCA) achieved

the best performance across all datasets: training set macro-AUC = 0.842 (95% CI: 0.786-0.898), internal validation = 0.811 (0.703-0.906), external validation = 0.817 (0.679–0.935); ACC = 0.635, 0.695, 0.520; macro-F1 = 0.636, 0.672, 0.507, respectively.

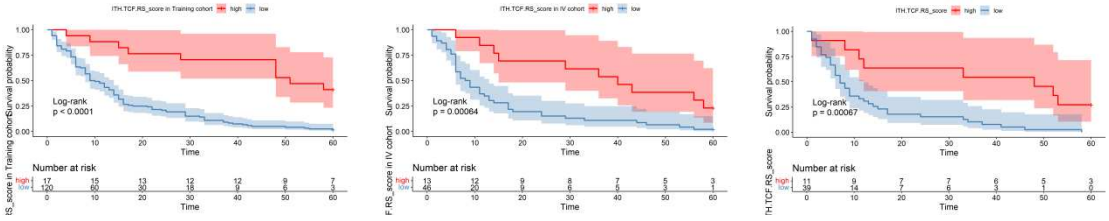
Among the single-modality models, the ITH model performed the best (external AUC = 0.731), outperforming RS (0.581) and BCA (0.644), whereas the clinical model performed the weakest (0.643). Among the two-modality models, the RS + ITH (external AUC = 0.795) and ITH + Clinical (0.763) models were better than the other combinations. The three-modality model (RS + ITH + BCA) achieved an external AUC of 0.800, second only to the full-dimensional model.

### 3.4 Kaplan–Meier curves and time-dependent ROC

Based on the risk stratification from the full-dimensional model (high-risk = predicted short-term; low-risk = predicted medium/long-term), Kaplan-Meier curves (Figure 3) in all three cohorts demonstrated significantly better OS for the low-risk group than the high-risk group (training: Log-rank $p < 0.0001$; internal validation: $p = 0.00064$; external validation: $p = 0.00067$). At 60 months, the OS rates for the low-risk groups were > 40%, ~20%, and ~25%, whereas those for the high-risk groups approached 0%, confirming the robust survival stratification ability of the model.

Time-dependent ROC curves (Figure 4) for predicting 3-year long-term sur

vival yielded AUCs of 0.850 (training), 0.790 (internal validation), and 0.760 (external validation), with a drop of < 0.1 between training and external sets, indicating good generalizability.




A. Kaplan-Meier Survival Curve of the training set

B. Kaplan-Meier Survival Curve of the Internal test set

C. Kaplan-Meier Survival Curve of the External test set

**Figure 3. Kaplan–Meier survival curves of the full-dimensional fusion model**

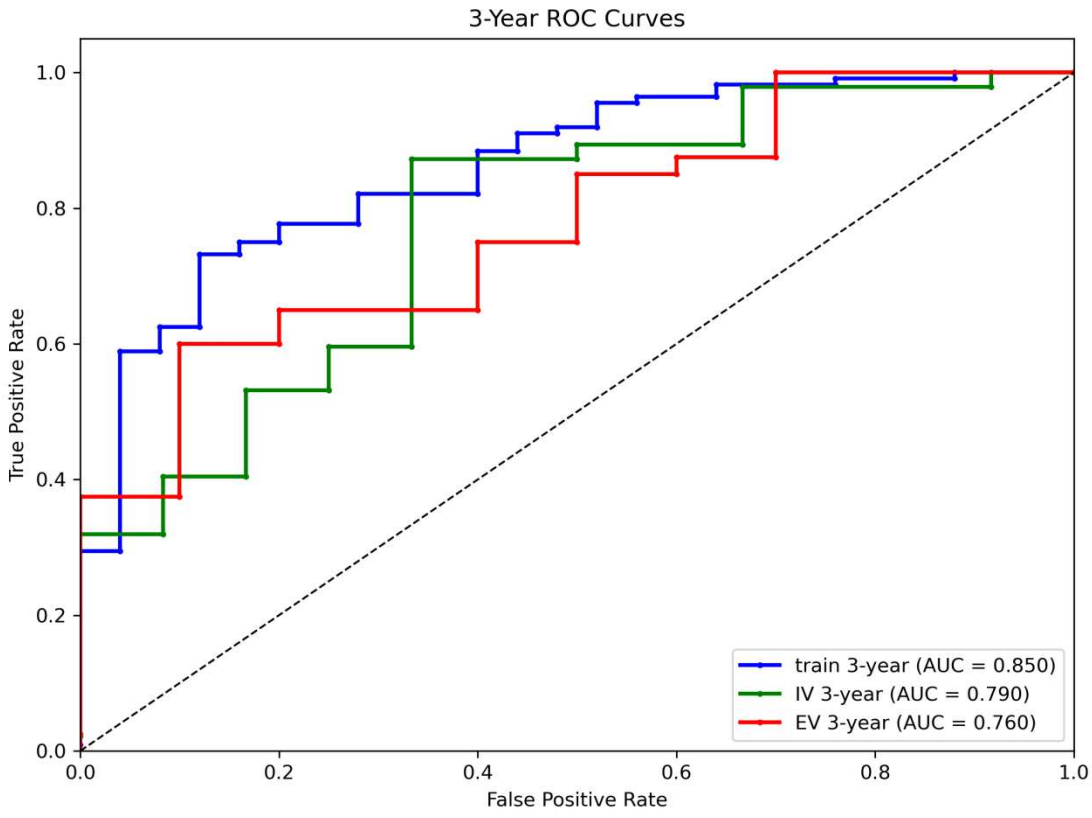


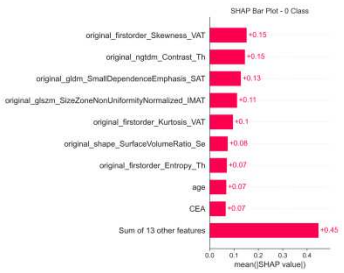

**Figure 4. Time-dependent receiver operating characteristic (ROC) curves of**

**the full-modality fusion model**

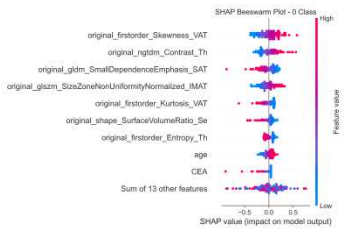
To evaluate the discriminative performance of the radiomic signature for 3-year survival outcomes (overall survival/progression-free survival selected according to study design) across three independent cohorts, time-dependent ROC curves were generated.

### 3.5 Model interpretability

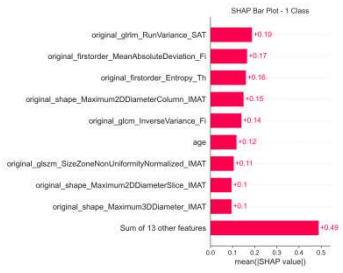
The SHAP analysis (Figure 5) revealed that BCA features contributed the most across all three prediction classes. For short-term survival prediction, visceral adipose tissue (VAT) skewness and tumor NGTDM contrast were the most important (mean absolute SHAP = 0.15 each), followed by SAT small dependence emphasis (0.13) and IMAT size-zone non-uniformity (0.11); clinical features (age and CEA) each had a contribution of 0.07. For medium-term prediction, SAT run variance was the most important (0.19), followed by tumor entropy (0.16) and IMAT maximum 2D diameter (0.15). For long-term prediction, the first-order mean absolute deviation (0.21), age (0.19), SAT small dependence emphasis (0.18), and IMAT maximum 2D diameter (0.17) were the top contributors, with relatively balanced contributions from other features, suggesting that long-term prognosis is comprehensively influenced by multiple factors.



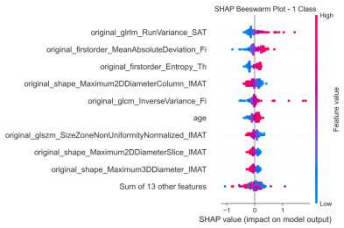

A. Bar Plot for the Short-Term Survival Group



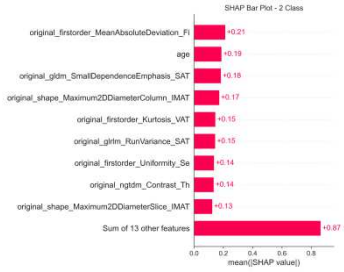

B. Beeswarm Plot for the Short-Term Survival Group



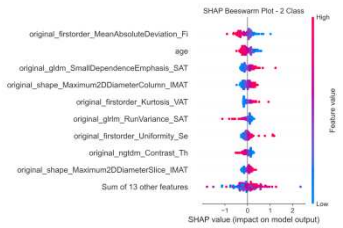

C. Bar Plot for the Intermediate-Term Survival Group




D. Beeswarm Plot for the Intermediate-Term Survival Group




E. Bar Plot for the Long-Term Survival Group




F. Beeswarm Plot for the Long-Term Survival Group

**Figure 5. SHapley Additive exPlanations (SHAP) plots of the full-dimension al fusion model**

## 4 Discussion

In this study, we constructed and validated a multi-dimensional Cox-based prognostic model integrating ITH, BCA, RS, and clinical features (CLIC). Beca use OS is a time-to-event endpoint, Cox proportional hazards models were use d as the primary analytical approach, allowing censored patients to be handled appropriately and preserving survival time information. The fusion model combi

ning clinical, radiomics, tumor habitat, and body composition features demonstrated optimal predictive performance, with C-index values of 0.850 in the training, 0.790 in the internal test, and 0.760 in the external test sets; these two metrics reflect different aspects of model performance and are reported separately. with AUCs of 0.842 (training), 0.811 (internal test), and 0.817 (external test), It outperformed single-modality models (clinical-only external time-dependent AUC: 0.643). Kaplan-Meier analysis confirmed significant risk stratification between high- and low-risk groups (log-rank p = 0.00067). The model achieved C-indices of 0.850, 0.790, and 0.760 across cohorts, supporting a robust "tumor-host" integrated prognostic framework for stage IV NSCLC. Compared with existing radiomics approaches that rely on whole-tumor feature extraction and often obscure spatial heterogeneity [10,11,12,14], our findings demonstrate the advantage of incorporating multi-dimensional tumor and host information into survival prediction.

Our results extend prior literature by introducing habitat-based imaging for spatial deconvolution of the tumor microenvironment, enabling quantification of intratumoral niches defined by intensity, texture, and morphological variation [12,13,15]. These habitat features may correlate with high-risk histopathological patterns, including micropapillary/solid components and immune-depleted regions [14,15], capturing key determinants of overall survival [16,18]. This approach improved predictive performance compared with prior single-modality models; for example, Kim et al. [22] reported a C-index of 0.78 using tumor burden-

based features without spatial heterogeneity , highlighting the incremental value of habitat-driven modeling. In addition, our findings support a shift from tumor-centric prognostic frameworks to a combined “seed and soil” paradigm integrating tumor aggressiveness and host metabolic reserve [17,19].

In stage IV NSCLC treated with immunotherapy and chemotherapy, outcomes are determined not only by tumor biology (ITH, RS) but also by host nutritional and inflammatory status [17,18]. By incorporating body composition parameters, including skeletal muscle and adipose distribution, we captured host metabolic reserve as an independent and interacting prognostic factor [19,20]. Compared with models based solely on clinical or inflammatory markers (e.g., Xia et al. [25,26]), our multi-dimensional integration demonstrated superior discriminative ability. Clinically, this model addresses prognostic heterogeneity among patients with similar TNM stage and ECOG status, particularly those with occult radiological frailty such as sarcopenia that is not detectable by routine assessment but identifiable on CT imaging [32,33]. This enables early risk stratification and supports individualized interventions including nutritional support, prehabilitation, treatment adjustment, or intensified monitoring [34,35,36,37].

Despite these strengths, some limitations should be acknowledged. First, the sample size was relatively small compared with the large number of imaging and body composition features and the complexity of the modeling process. Although LASSO and cross-validation were used, the possibility of overfitting remains. In addition, the external validation cohort consisted of only 50 patients,

which limits the reliability of the external validation results. Radiomics and habitat features may be influenced by variability in CT acquisition parameters, including slice thickness and reconstruction algorithms, which may affect reproducibility across scanners [11,38]. Further prospective multicenter validation in heterogeneous real-world populations remains necessary [37]. Additionally, the model is based on baseline imaging and does not capture temporal changes in tumor biology or host status during treatment [28]. Future work should integrate longitudinal imaging with circulating tumor DNA analysis to enable dynamic monitoring of tumor evolution and resistance, potentially forming a spatiotemporal multi-omics framework for improved prognostication in NSCLC [28,38].

## Declarations

### Ethics approval and consent to participate

The research protocol was approved by the Ethics Committee of Panzhihua Traditional Chinese Medicine and Western Medicine Hospital (approval number: PCWEC-C-005). Given the retrospective nature of this study, the requirement for informed consent was waived. All methods were carried out in accordance with relevant guidelines and regulations. Our study adhered to the principles of the Declaration of Helsinki.

Human Ethics and Consent to Participate declarations: The informed consent was waived by the Ethics Committee of Panzhihua Traditional Chinese Medicine and Western Medicine Hospital for this retrospective study..

### Clinical trial number

Not Applicble.

**Consent for publication**

Not Applicable.

**Availability of data and materials**

The datasets generated and/or analysed during the current study are not publicly available due to privacy or ethical restrictions but are available from the corresponding author on reasonable request..

**Competing interests**

The authors declare no competing interests.

**Funding**

This work was supported by the Program for 2023 Kunming Health Science and Technology Talent Training Project (Medical Technology Center) (No.2023-SW-13）. National Natural Science Foundation of China (NSFC)(No.82160348)，2024 Senior Health Technology and Medical Discipline Leader of Yunnan Provincial Health Commission(No. D-2024056).

**Authors' contributions**

PQW, HH, YBW ,YDY and YF contributed equally to the study concept and design, acquisition of subjects and data, analysis and interpretation of data, and preparation of the manuscript and need therefore be granted both first authorship.BSX and JGL were involved in the study design, data analysis and interpretation, and manuscript review. MXK contributed to the study design and manuscript review. CYW participated in the study design, data analysis and interpretation, and manuscript preparation. LY assisted in data acquisition and reviewed the manuscript. DMY contributed to the revision of the article and the communication and collaboration within the team.BY was involved in the study design, data collection, data analysis and interpretation, and manuscript preparation. All the

authors read and approved the final manuscript.

**Acknowledgements**

We thank Panzhihua Traditional Chinese Medicine and Western Medicine Hospital and Panzhihua Central Hospital for providing data records.

**Abbreviations**

NSCLC: Non-small cell lung cancer

OS: Overall survival

CT: Computed tomography

ROI: Region of interest

ICC: Intraclass correlation coefficient

RS: Radiomics

ITH: Intratumoral heterogeneity

BCA: Body composition analysis

LASSO: Least absolute shrinkage and selection operator

CLIC: Clinical

AUC: Area under the curve

ROC: Receiver operating characteristic

SHAP: SHapley Additive exPlanations

VAT: Visceral adipose tissue

SAT: Subcutaneous adipose tissue

IMAT: Intermuscular adipose tissue

SMI: Skeletal muscle index

PD-L1: Programmed death-ligand 1

## References


[1]. Sung H, Ferlay J, Siegel RL, Laversanne M, Soerjomataram I, Jemal A, Bray F. Global cancer statistics 2020: GLOBOCAN estimates of incidence and mortality worldwide for 36 cancers in 185 countries. CA Cancer J Clin. 2021;71(3):209-249. doi:10.3322/caac.21660. Epub February 4, 2021. PMID:33538338.

[2]. Wagle NS, Nogueira L, Devasia TP, Mariotto AB, Yabroff KR, Islami F, Jemal A, Alteri R, Ganz PA, Siegel RL. Cancer treatment and survivorship statistics, 2025. CA Cancer J Clin. 2025;75(4):308-340. doi:10.3322/caac.70011. Epub May 30, 2025. Erratum in: CA Cancer J Clin. 2025;75(6):683. doi:10.3322/caac.70036. PMID:40445120; PMCID:PMC12223361.

[3]. Fong KM, Rosenthal A, Giroux DJ, Nishimura KK, Erasmus J, Lievens Y, Marino M, Marom EM, Putora PM, Singh N, Suárez F, Rami-Porta R, Detterbeck F, Eberhardt WEE, Asamura H; Members of the International Association for the Study of Lung Cancer Staging and Prognostic Factors Committee, Members of the Advisory Boards, and Participating Institutions of the Lung Cancer Domain. The International Association for the Study of Lung Cancer staging project for lung cancer: proposals for the revision of the M descriptors in the forthcoming ninth edition of the TNM classification for lung cancer. J Thorac Oncol. 2024;19(5):786-802. doi:10.1016/j.jtho.2024.01.019. Epub February 4, 2024. Erratum in: J Thorac Oncol. 2025;20(4):531. doi:10.1016/j.jtho.20

25.01.017. PMID:38320664.

[4]. Yang JC, Lu S, Hayashi H, Felip E, Spira AI, Girard N, Kim YJ, Lee SH, Ostapenko Y, Danchaivijitr P, Liu B, Alip A, Korbenfeld E, Mourão Dias J, Besse B, Passaro A, Lee KH, Xiong H, How SH, Cheng Y, Chang GC, Yoshioka H, Thomas M, Nguyen D, Ou S I, Mukhedkar S, Prabhash K, D'Arcangelo M, Alatorre-Alexander J, Vázquez Limón JC, Alves S, Stroyakovskiy D, Peregudova M, Şendur MAN, Yazici O, Califano R, Gutiérre z Calderón V, de Marinis F, Kim SW, Gadgeel SM, Owen S, Xie J, Sun T, Mehta J, V enkatasubramanian R, Ennis M, Fennema E, Daksh M, Roshak A, Man J, Knoblauch RE, Bauml JM, Baig M, Shah S, Sethi S, Cho BC; MARIPOSA Investigators. Overall su rvival with amivantamab-lazertinib in EGFR-mutated advanced NSCLC. N Engl J Med. 2025;393(17):1681-1693. doi:10.1056/NEJMoa2503001. Epub September 7, 2025. PMI D:40923797.

[5]. Jänne PA, Planchard D, Kobayashi K, Yang JC, Liu Y, Valdiviezo N, Kim TM, Jiang L, K agamu H, Yanagitani N, Wang J, Biswas B, Poltoratskiy A, Neron Y, Rojas C, Koubkov a L, Escriu C, Ezeife DA, Mann H, Armenteros-Monterroso E, Rukazenkov Y, Lee CK; FLAURA2 Investigators. Survival with osimertinib plus chemotherapy in EGFR-mutated advanced NSCLC. N Engl J Med. 2026;394(1):27-38. doi:10.1056/NEJMoa2510308. Ep ub October 17, 2025. PMID:41104938.

[6]. Fang W, Wu L, Meng X, Yao Y, Zuo W, Yao W, Xie Y, Zhang Y, Cui J, Zhang Y, Li X, Zhuang W, Fang J, Wang Q, Jiang W, Li K, Bai Y, Luo Y, Ma F, Yu Y, Zheng W, Liu Z, Yang B, Ma R, Fang Y, Yang R, Jiang L, Hu J, Yang J, Diao Y, Jin X, Ge J, Yang Y, Zhang L. Sacituzumab tirumotecan in EGFR-TKI-resistant, EGFR-mutated advanced NS

CLC. N Engl J Med. 2026;394(1):13-26. doi:10.1056/NEJMoa2512071. Epub October 19, 2025. PMID:41124220.

[7]. Doroshow DB, Bhalla S, Beasley MB, Sholl LM, Kerr KM, Gnjatic S, Wistuba II, Rimm DL, Tsao MS, Hirsch FR. PD-L1 as a biomarker of response to immune-checkpoint inhibitors. Nat Rev Clin Oncol. 2021;18(6):345-362. doi:10.1038/s41571-021-00473-5. Epub February 12, 2021. PMID:33580222.

[8]. Horn L, Mansfield AS, Szczęsna A, Havel L, Krzakowski M, Hochmair MJ, Huemer F, Losonczy G, Johnson ML, Nishio M, Reck M, Mok T, Lam S, Shames DS, Liu J, Ding B, Lopez-Chavez A, Kabbinavar F, Lin W, Sandler A, Liu SV; IMpower133 Study Group. First-line atezolizumab plus chemotherapy in extensive-stage small-cell lung cancer. N Engl J Med. 2018;379(23):2220-2229. doi:10.1056/NEJMoa1809064. Epub September 25, 2018. PMID:30280641.

[9]. Marusyk A, Almendro V, Polyak K. Intra-tumour heterogeneity: a looking glass for cancer? Nat Rev Cancer. 2012;12(5):323-334. doi:10.1038/nrc3261. PMID:22513401.

[10].Lambin P, Rios-Velazquez E, Leijenaar R, Carvalho S, van Stiphout RG, Granton P, Zegers CM, Gillies R, Boellard R, Dekker A, Aerts HJ. Radiomics: extracting more information from medical images using advanced feature analysis. Eur J Cancer. 2012;48(4):441-446. doi:10.1016/j.ejca.2011.11.036. Epub January 16, 2012. PMID:22257792; PMCID:PMC4533986.

[11].Mazzaschi G, Marrocchio C, Moron Dalla Tor L, Leo L, Balbi M, Milanese G, Adebanjo GAR, Lorusso B, Monica G, Pluchino M, Minari R, D'Agnelli S, Cardinale E, Perrone F, Bordi P, Leonetti A, Ledda RE, Silva M, Buti S, Roti G, Bettati S, Quaini F, Tise

o M, Sverzellati N. Longitudinal blood immune-inflammatory and radiomic profiling to decode different patterns of acquired resistance to immunotherapy in patients with NSCLC. Clin Cancer Res. 2025;31(8):1533-1545. doi:10.1158/1078-0432.CCR-24-1926. PMID:39670974.

[12].Shang Y, Zeng Y, Luo S, Wang Y, Yao J, Li M, Li X, Kui X, Wu H, Fan K, Li ZC, Zheng H, Li G, Liu J, Zhao W. Habitat imaging with tumoral and peritumoral radiomics for prediction of lung adenocarcinoma invasiveness on preoperative chest CT: a multicenter study. AJR Am J Roentgenol. 2024;223(4):e2431675. doi:10.2214/AJR.24.31675. Epub August 14, 2024. PMID:39140631.

[13].Huang X, Huang X, Xie Y, Wang K, Bai H, Ning R, Zhu X, Huang D, Jin G. Integrative habitat analysis and multi-instance deep learning for predictive model of PD-1/PD-L1 immunotherapy efficacy in NSCLC patients: a dual-center retrospective study. BMC Med Imaging. 2025;25(1):288. doi:10.1186/s12880-025-01828-5. PMID:40676504; PMCID:PMC12272984.

[14].Huang S, Liang X, Lou K, Zhou J, Wang J, Xu G, Wu S, Hu H, Dong H. Comparing habitat, radiomics, and fusion models for predicting micropapillary/solid components in stage I lung adenocarcinoma. Acad Radiol. 2025;32(10):6307-6319. doi:10.1016/j.acra.2025.07.035. Epub July 31, 2025. PMID:40750538.

[15].Park S, Ock CY, Kim H, Pereira S, Park S, Ma M, Choi S, Kim S, Shin S, Aum BJ, Paeng K, Yoo D, Cha H, Park S, Suh KJ, Jung HA, Kim SH, Kim YJ, Sun JM, Chung JH, Ahn JS, Ahn MJ, Lee JS, Park K, Song SY, Bang YJ, Choi YL, Mok TS, Lee SH. Artificial intelligence-powered spatial analysis of tumor-infiltrating lymphocytes as comple

mentary biomarker for immune checkpoint inhibition in non-small-cell lung cancer. J Clin Oncol. 2022;40(17):1916-1928. doi:10.1200/JCO.21.02010. Epub March 10, 2022. PMID:35271299; PMCID:PMC9177249.

[16].Geng Z, Hu Y, Zhou S, Wu G, Gong Z, Feng R, Huang Z, Mei P, Li K, Ye G, Liao Y. Prediction of tumor-infiltrating lymphocytes through habitat radiomics and exploration of response mechanisms in neoadjuvant immunochemotherapy-treated lung cancer. Cancer Immunol Immunother. 2026;75(2):42. doi:10.1007/s00262-025-04291-x. PMID:41591567; PMCID:PMC12847592.

[17].Fearon K, Strasser F, Anker SD, Bosaeus I, Bruera E, Fainsinger RL, Jatoi A, Loprinzi C, MacDonald N, Mantovani G, Davis M, Muscaritoli M, Ottery F, Radbruch L, Ravasco P, Walsh D, Wilcock A, Kaasa S, Baracos VE. Definition and classification of cancer cachexia: an international consensus. Lancet Oncol. 2011;12(5):489-495. doi:10.1016/S1470-2045(10)70218-7. Epub February 4, 2011. PMID:21296615.

[18].Argilés JM, López-Soriano FJ, Stemmler B, Busquets S. Cancer-associated cachexia - understanding the tumour macroenvironment and microenvironment to improve management. Nat Rev Clin Oncol. 2023;20(4):250-264. doi:10.1038/s41571-023-00734-5. Epub February 20, 2023. PMID:36806788.

[19].Decazes P, Ammari S, Belkouchi Y, Mottay L, Lawrance L, de Prévia A, Talbot H, Farhane S, Cournède PH, Marabelle A, Guisier F, Planchard D, Ibrahim T, Robert C, Barlesi F, Vera P, Lassau N. Synergic prognostic value of 3D CT scan subcutaneous fat and muscle masses for immunotherapy-treated cancer. J Immunother Cancer. 2023;11(9):e007315. doi:10.1136/jitc-2023-007315. PMID:37678919; PMCID:PMC10496660.

[20].Ha NB, Fan B, Shui AM, Huang CY, Brandman D, Lai JC. CT-quantified sarcopenic visceral obesity is associated with poor transplant waitlist mortality in patients with cirrhosis. Liver Transpl. 2023;29(5):476-484. doi:10.1097/LVT.0000000000000010. Epub January 3, 2023. PMID:36735830; PMCID:PMC10193893.

[21].Pecci F, Mazzaschi G, Dodi A, Tamarozzi P, Manini M, Peroni M, D'Agnelli S, Moron Dalla Tor L, Bruschi G, Pluchino M, Verzè M, Minari R, Perrone F, Bordi P, Leonetti A, Quaini F, Sverzellati N, Buti S, Tiseo M. Dissecting the impact of Controlling Nutritional Status (CONUT) score on survival outcomes and immune-inflammatory profiles in patients with advanced NSCLC undergoing first-line immunotherapy. J Immunother Cancer. 2026;14(1):e013045. doi:10.1136/jitc-2025-012205. PMID:41494746; PMCID:PMC12778215.

[22].Kim Y, Lee J, Chamseddine I, Grassberger C, Yoon HI, Kim KH, Cho Y, Sung W. Personalized survival models for choosing irradiated tumor burden on combined radiotherapy and immune checkpoint inhibitors in stage IV NSCLC patients. Phys Med. 2026;143:105751. doi:10.1016/j.ejmp.2026.105751. Epub February 20, 2026. PMID:41722292.

[23].Tran TN, Fong C, Pichotta K, Luthra A, Shen R, Chen Y, Waters M, Kim S, Li X, de Bruijn I, Riely G, Berger MF, Ladanyi M, Chakravarty D, Schultz N, Jee J. AI cancer driver mutation predictions are valid in real-world data. Nat Commun. 2025;16(1):8509. doi:10.1038/s41467-025-63461-8. PMID:41006257; PMCID:PMC12474978.

[24].Wang X, Ricciuti B, Elkrief A, Alessi JV, Di Federico A, Pecci F, Nishino M, Gulhan D, Ananda G, Rodig SJ, Sholl L, Johnson B, Lin X, Schoenfeld A, Awad MM, Christiani D. Multi-omics analysis reveals differential benefits of immunotherapy±chemotherapy

based on detailed smoking history in advanced non-small cell lung cancer. J Immun other Cancer. 2025;13(12):e012205. doi:10.1136/jitc-2025-012205. PMID:41423267; PMCID:PMC12719888.

[25].Xia J, Pang Y, Yang Y, Teng J, Lin Q. A tale of two periods: the evolution of determinants and CVD mortality risk in metastatic NSCLC. Rev Cardiovasc Med. 2025;26(9):39296. doi:10.31083/RCM39296. PMID:41089791; PMCID:PMC12516739.

[26].Zhang Y, Liu S, Chen J, Chen R, Yang Z, Sheng R, Li X, Wang T, Liu H, Yang F, Ying J, Yang L, Sun J, Zhou M. Deep learning-based histomorphological subtyping and risk stratification of small cell lung cancer from hematoxylin and eosin-stained whole slide images. Genome Med. 2025;17(1):98. doi:10.1186/s13073-025-01526-5. PMID:40898302; PMCID:PMC12406473.

[27].Sujit SJ, Aminu M, Karpinets TV, Chen P, Saad MB, Salehjahromi M, Boom JD, Qayati M, George JM, Allen H, Antonoff MB, Hong L, Hu X, Heeke S, Tran HT, Le X, Elamin YY, Altan M, Vokes NI, Sheshadri A, Lin J, Zhang J, Lu Y, Behrens C, Godoy MCB, Wu CC, Chang JY, Chung C, Jaffray DA, Wistuba II, Lee JJ, Vaporciyan AA, Gibbons DL, Heymach J, Zhang J, Cascone T, Wu J. Enhancing NSCLC recurrence prediction with PET/CT habitat imaging, ctDNA, and integrative radiogenomics-blood insights. Nat Commun. 2024;15(1):3152. doi:10.1038/s41467-024-47512-0. PMID:38605064; PMCID:PMC11009351.

[28].Guldbrandsen KF, Bloch M, Skougaard K, Ahlborn LB, Jakobsen E, Højsgaard A, Petersen RH, Møller LB, Dahl M, Sorensen BS, Frank MS, Ehlers JH, Krakauer M, Gørtz PM, Albrecht-Beste E, Grüner JM, Saghir Z, Fledelius J, Nielsen AL, Holdgaard PC, Niel

sen SS, Pøhl M, Borissova S, Land LH, Kristiansen C, McCulloch T, Mortensen LS, Nellemann HM, Christophersen MS, Hilberg O, Rasmussen TL, Schwaner SHS, Laursen CB, Bodtger U, Sopina L, Lonsdale MN, Meyer CN, Gerke O, Mortensen J, Rasmussen TR, Fischer BM; SUPE_R Study Group. Surveillance with fluorine-18 fluorodeoxyglucose positron emission tomography/computed tomography of patients with stage I-to-III lung cancer after completion of curative treatment (SUPE_R): a randomized controlled trial. J Thorac Oncol. 2025;20(8):1086-1097. doi:10.1016/j.jtho.2025.04.003. Epub April 19, 2025. Erratum in: J Thorac Oncol. 2026;21(5):103558. doi:10.1016/j.jtho.2026.103558. PMID:40258572.

[29].Cortellini A, Brunetti L, Di Fazio GR, Garbo E, Pinato DJ, Naidoo J, Katz A, Loza M, Neal JW, Genova C, Gettinger S, Kim SY, Jayakrishnan R, El Zarif T, Russano M, Pecci F, Di Federico A, Awad M, Alessi JV, Montrone M, Owen DH, Signorelli D, Fidler MJ, Li M, Camerini A, De Giglio A, Young L, Vincenzi B, Metro G, Passiglia F, Yendamuri S, Guida A, Ghidini M, Awosika NO, Napolitano A, Fulgenzi CAM, Grisanti S, Grossi F, D'Incecco A, Josephides E, Van Hemelrijck M, Russo A, Gelibter A, Spinelli G, Verrico M, Tomasik B, Giusti R, Newsom-Davis T, Bria E, Sebastian M, Rost M, Forster M, Mukherjee U, Landi L, Mazzoni F, Aujayeb A, Dupont M, Curioni-Fontecedro A, Chiari R, Pantano F, Morabito A, Leonetti A, Friedlaender A, Addeo A, Zoratto F, De Tursi M, Cantini L, Roca E, Mountzios G, Della Gravara L, Kalvapudi S, Inno A, Bironzo P, Di Marco Barros R, O'Reilly D, Bell J, Karapanagiotou E, Monnet I, Baena J, Macerelli M, Majem M, Agustoni F, Cortinovis DL, Tonini G, Minuti G, Bennati C, Mezquita L, Gorría T, Servetto A, Beninato T, Lo Russo G, Rogado J, Moliner L, Biel

lo F, Aboubakar Nana F, Dingemans AM, Aerts JGJV, Ferrara R, Torri V, Hejleh TA, Takada K, Naqash AR, Garassino M, Peters S, Wakelee H, Nassar AH, Ricciuti B. Determinants of 5-year survival in patients with advanced NSCLC with PD-L1⩾50% treated with first-line pembrolizumab outside of clinical trials: results from the Pembro-real 5Y global registry. J Immunother Cancer. 2025;13(2):e010674. doi:10.1136/jitc-2024-010674. PMID:39904562; PMCID:PMC11795382.

[30].Wu LX, Ding N, Ji YD, Zhang YC, Li MJ, Shen JC, Hu HT, Jin L, Yin SN. Habitat analysis in tumor imaging: advancing precision medicine through radiomic subregion segmentation. Cancer Manag Res. 2025;17:731-741. doi:10.2147/CMAR.S511796. PMID:40190416; PMCID:PMC11971994.

[31].Kather JN, Pearson AT, Halama N, Jäger D, Krause J, Loosen SH, Marx A, Boor P, Tacke F, Neumann UP, Grabsch HI, Yoshikawa T, Brenner H, Chang-Claude J, Hoffmeister M, Trautwein C, Luedde T. Deep learning can predict microsatellite instability directly from histology in gastrointestinal cancer. Nat Med. 2019;25(7):1054-1056. doi:10.1038/s41591-019-0462-y. Epub June 3, 2019. PMID:31160815; PMCID:PMC7423299.

[32].Shachar SS, Deal AM, Weinberg M, Nyrop KA, Williams GR, Nishijima TF, Benbow JM, Muss HB. Skeletal muscle measures as predictors of toxicity, hospitalization, and survival in patients with metastatic breast cancer receiving taxane-based chemotherapy. Clin Cancer Res. 2017;23(3):658-665. doi:10.1158/1078-0432.CCR-16-0940. Epub August 3, 2016. PMID:27489287; PMCID:PMC5290138.

[33].Tamir S, Behar HV, Tal R, Jasper RT, Armoni M, Aloni HP, Orad RI, Voet H, Atar E, Grubstein A, Stemmer SM, Markel G. CT body composition changes predict survival

in immunotherapy-treated cancer patients: a retrospective cohort study. Cancers (Basel). 2026;18(2):341. doi:10.3390/cancers18020341. PMID:41595260; PMCID:PMC12839126.

[34].Mitra J, Ghose S, Thawani R. Clinically explainable prediction of immunotherapy response integrating radiomics and clinico-pathological information in non-small cell lung cancer. Cancers (Basel). 2025;17(16):2679. doi:10.3390/cancers17162679. PMID:40867308; PMCID:PMC12384141.

[35].Ji Y, Cui K, Zhang J, Wang J, Dai Z, Cui Y, Ge H, Zheng J, Yu D. Noninvasive prediction of programmed cell death protein-ligand 1 expression in locally advanced non-small cell lung cancer by 18F-fluorodeoxyglucose positron emission tomography/computed tomography-based metabolic habitats: a multicenter radiomic and biological study. Ann Surg Oncol. 2025;32(13):10094-10107. doi:10.1245/s10434-025-18139-2. Epub August 29, 2025. PMID:40883535; PMCID:PMC12589310.

[36].Berenguer R, Pastor-Juan MDR, Canales-Vázquez J, Castro-García M, Villas MV, Mansilla Legorburo F, Sabater S. Radiomics of CT features may be nonreproducible and redundant: influence of CT acquisition parameters. Radiology. 2018;288(2):407-415. doi:10.1148/radiol.2018172361. Epub April 24, 2018. PMID:29688159.

[37].Moding EJ, Shahrokh Esfahani M, Jin C, Hui AB, Nabet BY, Liu Y, Chabon JJ, Binkley MS, Kurtz DM, Hamilton EG, Chaudhuri AA, Liu CL, Li Z, Bonilla RF, Jiang AL, Lau BC, Lopez P, He J, Qiao Y, Xu T, Yao L, Gandhi S, Liao Z, Das M, Ramchandran KJ, Padda SK, Neal JW, Wakelee HA, Gensheimer MF, Loo BW Jr, Li R, Lin SH, Alizadeh AA, Diehn M. Integrating ctDNA analysis and radiomics for dynamic risk assessment

in localized lung cancer. Cancer Discov. 2025;15(8):1609-1629. doi:10.1158/2159-8290.CD-24-1704. PMID:40299851; PMCID:PMC12324966.

[38]. Ahmed HM, Al-Hussainy AF, Mustafa WW, Jyothi SR, Nayak PP, Janney JB, Singh G, Sinha A, Sameer HN, Salih RM, Adil M, Salajegheh P. Circulating tumor DNA dynamics predict pathological response and guide therapy personalization in the neoadjuvant setting. Discov Oncol. 2026;17(1):365. doi:10.1007/s12672-026-04495-2. PMID:41611911; PMCID:PMC12936245.

**Attachement（table）**

### 3.3 Model performance

**Table 2. Performance metrics of all models**

| Model name | Dataset | macro-AUC (95% CI) | ACC | macro-SEN | macro-SPE | macro-F1 |
|---|---|---|---|---|---|---|
| Full-dimensional Combined model | Training set | 0.842 (0.786, 0.898) | 0.635 | 0.702 | 0.807 | 0.636 |
| | Internal test set | 0.811 (0.703, 0.906) | 0.695 | 0.762 | 0.866 | 0.672 |
| | External test set | 0.817 (0.679, 0.935) | 0.520 | 0.607 | 0.757 | 0.507 |
| ITH + RS + BCA model | Training set | 0.783 (0.719, 0.845) | 0.620 | 0.635 | 0.794 | 0.586 |
| | Internal test set | 0.809 (0.734, 0.884) | 0.610 | 0.651 | 0.784 | 0.594 |
| | External test set | 0.800 (0.683, 0.898) | 0.600 | 0.647 | 0.802 | 0.565 |
| ITH + RS model | Training set | 0.782 (0.719, 0.841) | 0.628 | 0.653 | 0.796 | 0.603 |
| | Internal test set | 0.775 (0.636, 0.879) | 0.729 | 0.794 | 0.878 | 0.717 |

| | | | | | | |
|---|---|---|---|---|---|---|
| | External tes | 0.795 (0.687, 0.890) | 0.620 | 0.705 | 0.797 | 0.596 |
| ITH + CLIC model | Training set | 0.779 (0.715, 0.838) | 0.577 | 0.592 | 0.774 | 0.559 |
| | Internal test | 0.770 (0.666, 0.869) | 0.695 | 0.710 | 0.866 | 0.645 |
| | External tes | 0.763 (0.641, 0.863) | 0.500 | 0.608 | 0.762 | 0.488 |
| ITH single-modality m | Training set | 0.737 (0.666, 0.802) | 0.606 | 0.606 | 0.784 | 0.556 |
| | Internal test | 0.722 (0.603, 0.830) | 0.661 | 0.607 | 0.779 | 0.576 |
| | External tes | 0.731 (0.590, 0.850) | 0.620 | 0.564 | 0.785 | 0.529 |
| BCA + CLIC model | Training set | 0.738 (0.666, 0.803) | 0.533 | 0.602 | 0.767 | 0.520 |
| | Internal test | 0.697 (0.597, 0.781) | 0.542 | 0.517 | 0.758 | 0.485 |
| | External tes | 0.702 (0.596, 0.802) | 0.500 | 0.543 | 0.762 | 0.467 |
| BCA single-modality | Training set | 0.736 (0.667, 0.794) | 0.489 | 0.537 | 0.745 | 0.469 |
| | Internal test | 0.665 (0.561, 0.786) | 0.559 | 0.558 | 0.761 | 0.528 |
| | External tes | 0.644 (0.511, 0.785) | 0.480 | 0.468 | 0.729 | 0.416 |
| Clinical single-modalit | Training set | 0.668 (0.591, 0.742) | 0.445 | 0.492 | 0.724 | 0.421 |
| | Internal test | 0.631 (0.507, 0.749) | 0.424 | 0.491 | 0.731 | 0.404 |
| | External tes | 0.643 (0.467, 0.802) | 0.440 | 0.476 | 0.726 | 0.402 |
| RS + CLIC model | Training set | 0.666 (0.588, 0.732) | 0.460 | 0.446 | 0.743 | 0.409 |
| | Internal test | 0.654 (0.514, 0.782) | 0.458 | 0.496 | 0.725 | 0.419 |
| | External tes | 0.591 (0.428, 0.726) | 0.460 | 0.458 | 0.696 | 0.403 |
| RS single-modality m | Training set | 0.625 (0.549, 0.706) | 0.526 | 0.431 | 0.726 | 0.396 |

| | | | | | |
|---|---|---|---|---|---|
| Internal test | 0.601 (0.468, 0.731) | 0.525 | 0.397 | 0.708 | 0.364 |
| External tes | 0.581 (0.417, 0.731) | 0.520 | 0.320 | 0.694 | 0.320 |

Abbreviations: AUC, area under the curve; CI, confidence interval; ACC, accuracy; SEN, sensitivity; SPE, specificity; F1, F1 score; ITH, intratumoral heterogeneity; RS, radiomics score (radiomic signature); BCA, body composition analysis; CLIC, clinical characteristics.